NANO · MICRO small
www.small-journal.com

Reversible Shielding and Immobilization of Liposomes and Viral Vectors by Tailored Antibody-Ligand Interactions

*Oliver S. Thomas, Balder Rebmann, Matthias Tonn, Ivo C. Schirmeister, Sarah Wehrle, Jan Becker, Gabriel J. Zea Jimenez, Sebastian Hook, Sarah Jäger, Melissa Klenzendorf, Mateo Laskowski, Alexander Kaier, Gerhard Pütz, Matias D. Zurbriggen, Wilfried Weber, Maximilian Hörner, and Hanna J. Wagner**

Controlling the time and dose of nanoparticulate drug delivery by administration of small molecule drugs holds promise for efficient and safer therapies. This study describes a versatile approach of exploiting antibody-ligand interactions for the design of small molecule-responsive nanocarrier and nanocomposite systems. For this purpose, antibody fragments (scFvs) specific for two distinct small molecule ligands are designed. Subsequently, the surface of nanoparticles (liposomes or adeno-associated viral vectors, AAVs) is modified with these ligands, serving as anchor points for scFv binding. By modifying the scFvs with polymer tails, they can act as a non-covalently bound shielding layer, which is recruited to the anchor points on the nanoparticle surface and prevents interactions with cultured mammalian cells. Administration of an excess of the respective ligand triggers competitive displacement of the shielding layer from the nanoparticle surface and restores nanoparticle-cell interactions. The same principle is applied for developing hydrogel depots that can release integrated AAVs or liposomes in response to small molecule ligands. The liberated nanoparticles subsequently deliver their cargoes to cells. In summary, the utilization of different antibody-ligand interactions, different nanoparticles, and different release systems validates the versatility of the design concept described herein.

1. Introduction

Nanotechnology allows the upgrade of existing and clinically proven drugs with sophisticated delivery vehicles in order to optimize pharmacokinetic parameters and ameliorate toxicity. Since long circulation times have been shown to be beneficial for bioavailability,[1–3] nanocarriers are often modified to reduce the binding of opsonizing agents, such as complement proteins or antibodies, or the uptake by sentinel cells of the immune system, such as macrophages.[4] A common strategy relies on decorating the surface of nanoparticles with polymers such as polyethylene glycol (PEG), which reduces interactions with proteins and cells by steric, enthalpic, and entropic effects.[5] Similarly, nanoparticles can be protected by incorporating them into hydrogels, whose high water content and viscoelastic properties resemble those of living tissues, making them ideally suited for use

O. S. Thomas, B. Rebmann,[+] M. Tonn, I. C. Schirmeister, S. Wehrle, J. Becker, G. J. Zea Jimenez, S. Hook, S. Jäger, M. Klenzendorf, M. Laskowski, A. Kaier, W. Weber, M. Hörner, H. J. Wagner
Faculty of Biology II
University of Freiburg
79104 Freiburg, Germany
E-mail: hanna.wagner@biologie.uni-freiburg.de

The ORCID identification number(s) for the author(s) of this article can be found under https://doi.org/10.1002/smll.202105157.

[+]Present address: Lipoid GmbH, 67065 Ludwigshafen, Germany

DOI: 10.1002/smll.202105157

O. S. Thomas, B. Rebmann, M. Tonn, I. C. Schirmeister, S. Wehrle, J. Becker, G. J. Zea Jimenez, S. Hook, S. Jäger, M. Klenzendorf, M. Laskowski, A. Kaier, W. Weber, M. Hörner, H. J. Wagner
Signalling Research Centres BIOSS and CIBSS
University of Freiburg
79104 Freiburg, Germany

O. S. Thomas, W. Weber
Spemann Graduate School of Biology and Medicine (SGBM)
University of Freiburg
79104 Freiburg, Germany

G. Pütz
University Medical Center Freiburg
Institute for Clinical Chemistry
79106 Freiburg, Germany

M. D. Zurbriggen
Institute of Synthetic Biology and CEPLAS
Heinrich Heine University Düsseldorf
40225 Düsseldorf, Germany

H. J. Wagner
Department of Biosystems Science and Engineering – D-BSSE
ETH Zurich
Basel 4058, Switzerland

as drug depots.[6–8] This combination of nanoparticles and hydrogel depots gave rise to a new class of delivery systems, termed nanocomposite systems.[9–12]

However, both PEGylation and entrapment in hydrogel depots also prevent efficient internalization of the nanocarrier and its cargo by the intended target cells, and a balance must be found between specific versus efficient uptake. To address this challenge, systems have been developed which enable induced release and targeted delivery by employing sheddable PEG coatings, degradable particles, or dissolvable gels.[12–15] These systems can be tailored to flexibly respond to their environment, for instance to exogenous stimuli such as induced local heating, ultrasonication, targeted magnetic fields, or illumination with light of a specific wavelength.[16–18] However, these triggers place high demands on available equipment and the expertise of trained personnel. The usage of bioavailable and tolerable small molecules as exogenous triggers, on the other hand, would be a suitable alternative, and upon further development could eventually allow temporally precise and controlled release in response to administration of a trigger compound.

To date, a number of delivery systems responding to endogenous small molecule metabolites such as ATP, glucose, or lactate have been developed. Typically, this is achieved by incorporating (often protein- or aptamer-based) binding partners into the material. Presence of the trigger molecule leads to a physicochemical rearrangement within the material, affecting cargo release.[19–22]

However, these endogenous substances are permanently present in human physiology at considerable and fluctuating concentrations, and are therefore unsuitable to exogenously trigger responsive nanoparticle and nanocomposite systems. Instead, the putative trigger substances employed in such a design should i) possess an excellent clinical safety profile, ii) have no other targeted pharmacological effects, iii) distribute across many tissue types, iv) be rapidly excreted after use, v) not be present at high concentrations in a regular diet, and vi) (ideally) already be licensed for clinical use. Furthermore, the interaction between the trigger molecule and its binding partner must be highly specific to avoid unintended release.

Here, we conducted a proof-of-concept study to develop prototype systems in agreement with these requirements. We exploited the exquisite specificity of antibody-antigen pairs for the reversible recruitment of functionalized antibody fragments to ligand-coupled nanoparticles. By first fusing polymeric tails to the antibody fragments, they acted as a non-covalently bound shielding layer. This was competitively removed by the addition of free ligand acting as a trigger molecule and converting the nanoparticles to their free and accessible state.

We chose two well-suited small molecule ligands as prospective triggers: fluorescein, which does not occur in human physiology, but is clinically used as a safe contrast agent,[23] and biotin, a naturally occurring vitamin,[24] which is present in plasma at concentrations below 10 nM—too low to inadvertently trigger stimulus-responsive systems.[25] Moreover, both molecules are bioavailable after oral administration and exhibit low toxicity.[23,24,26,27]

As a complementary component, antibody fragments are ideal building blocks for stimulus-triggered systems because antibodies have been in clinical use for over three decades,[28,29] can be raised against virtually any molecule of interest, and have been successfully applied for the generation of stimulus-responsive hydrogels.[30] Since F_C effector functions such as immune cell receptor activation or complement binding are both unnecessary and undesirable for our intended application, we used single-chain variable fragments (scFvs). scFvs comprise only the variable V_H and V_L domains of an antibody connected by a flexible peptide linker and therefore are devoid of the F_C part. They retain the specificity and affinity for their antigen and are functional without glycosylation, making them amenable for efficient production in prokaryotic expression hosts.[31–33]

In this study, we applied the same versatile design principle for rendering both nanocarrier and nanocomposite systems stimulus-responsive to exogenous small trigger molecules. We designed scFvs specifically tailored to achieve desirable stability properties and affinity for the trigger molecules. Subsequently, we covalently attached the respective trigger molecules to the surface of nanoparticles, thus enabling their non-covalent decoration with the scFvs. We validated this design principle with two representative classes of nanoparticles: liposomes (a versatile type of carrier suitable for encapsulation of hydrophilic and lipophilic cargo) and adeno-associated viral vectors (AAVs, a vector system for gene therapy applications). By functionally modifying the scFvs with polymeric tails, they acted as a recruitable shielding layer, and we characterized the systems by quantifying the association with (for liposomes) or the transduction of (for AAVs) cultured mammalian cells in the shielded and triggered free states. Using star-shaped multi-arm PEG for functionalization, the scFvs could also act as a backbone of dissolvable hydrogels into which nanoparticles were actively incorporated. We characterized these gels by measuring nanoparticle release in the stable and dissolved states.

The usability of our versatile design principle for the development of both a controlled deshielding system and stimulus-responsive hydrogel depots for nanoparticles demonstrated the advantage of combining tailored antibody-antigen interactions with the design of nanoparticles for the development of next-generation delivery systems.

2. Results and Discussion

2.1. Non-Covalent Reversible Shielding of Nanoparticles

In this study, we propose a versatile strategy to control nanoparticle-cell interactions by modifying the surface of nanoparticles with small molecules, thus allowing their reversible interaction with functionally modified scFvs directed against these small molecules.

To confer shielding properties on the cognate scFvs, we genetically fused them to PAS tails, thus avoiding chemical coupling to PEG, which is often used for shielding. PAS is a synthetic polypeptide sequence named after its constituent monomers proline, alanine, and serine, which are arranged in a repetitive fashion.[34] PAS repeats adopt a random coil structure, exposing the hydrophilic backbone and mimicking the biophysical characteristics of PEG.[35] Upon binding to the ligands exposed on the nanoparticle surface, the PASylated scFvs acted

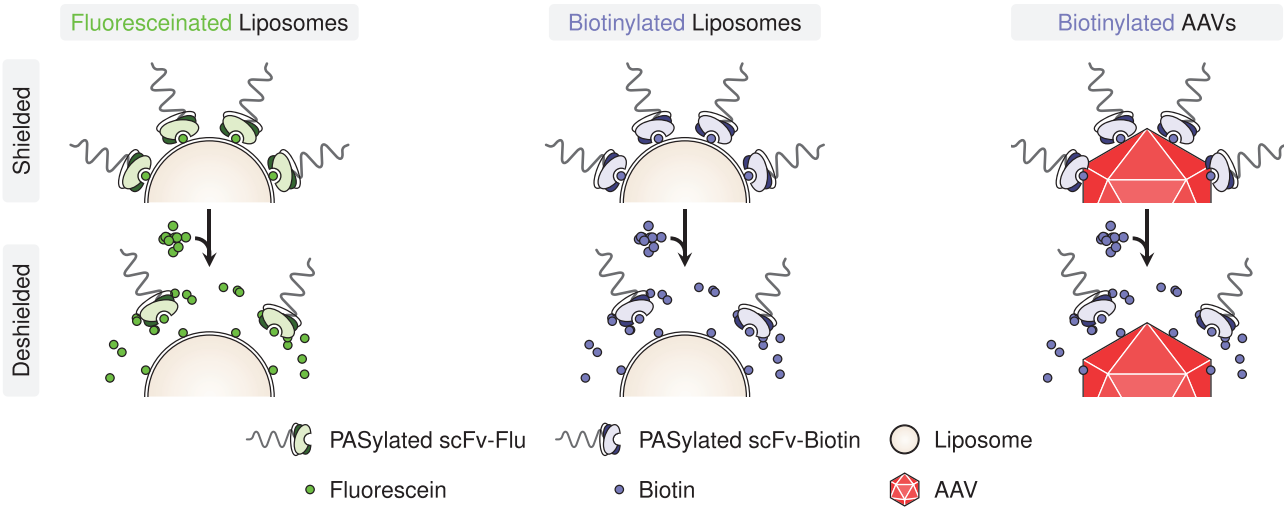

Figure 1. Shielding of liposomes or AAVs by exploitation of scFv-ligand interactions. Covalently modifying the surface of liposomes or AAVs with fluorescein or biotin allows their reversible decoration with specifically designed scFvs. By fusing the scFvs to a PAS tail (a polypeptide with biophysical properties similar to PEG), attachment of the scFvs to the nanoparticle surface results in *shielding* of the nanoparticles, preventing interaction with cells. Subsequent addition of the free ligand competes with the surface-attached ligand for binding to the scFv, resulting in *deshielding*. Illustrated components are not drawn to scale.

as a shielding layer. Since this interaction is reversible, addition of the free ligand competitively removed the scFvs, thus liberating the nanoparticle and enabling cell binding (**Figure 1**).

We first established the system exemplarily with liposomes whose deshielding could be controlled by fluorescein. We then verified the tailoring of the trigger ligand by generating biotin-responsive liposomes. Finally, we demonstrated the versatility of the approach by controlling the transduction of cells through biotin-responsive AAVs.

For the establishment of our system, we used empty liposomes with a lipid composition similar to that of Doxil (the clinically used PEGylated liposomal formulation of the anthracycline doxorubicin), but omitting the PEGylated lipid component (i.e., 60 mol% hydrogenated soy phosphatidyl choline (HSPC), 40 mol% cholesterol).[36] First, we investigated whether the presence of fluorescein (Flu) or biotin on the surface of liposomes would interfere with cellular association. For this purpose, we prepared liposomes marked with the fluorescent lipophilic tracer DiD and quantified their association with HeLa cells via flow cytometry (**Figure 2**A and Figure S1, Supporting Information). When comparing the area under the curves (AUCs) of cellular association over time for the different liposome species, modification with neither fluorescein nor biotin had a negative impact on cell association (AUCs of kinetic curves for modified liposomes compared

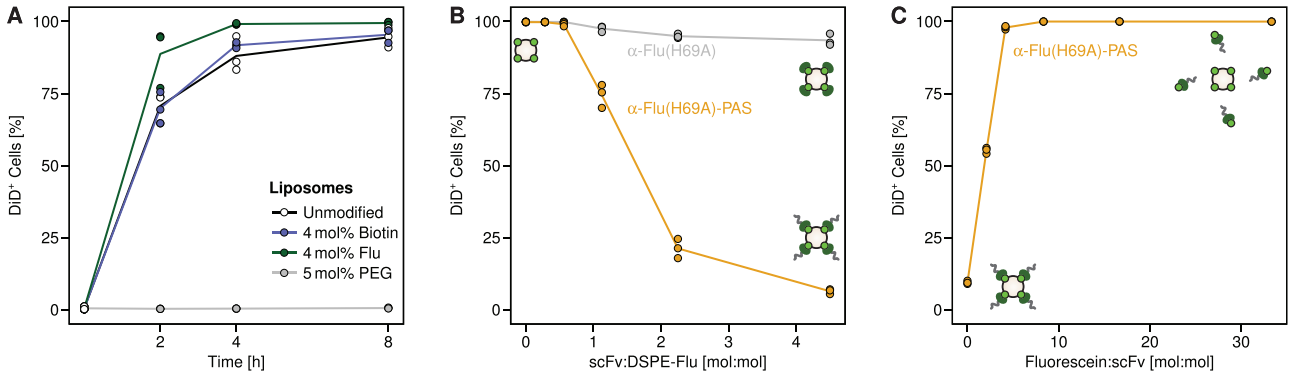

Figure 2. Shielding of fluorescein-modified liposomes by PASylated scFvs prevents association with cells. Liposomes labeled with the lipophilic fluorescent dye DiD are prepared and modified with 4 mol% distearoyl-phosphoethanolamine (DSPE)-Fluorescein, 4 mol% dipalmitoyl-phosphoethanolamine (DPPE)-Biotin, or 5 mol% DSPE-PEG2000. Liposomes (100 µM phospholipids, 167 µM total lipid) are incubated with HeLa cells and cell association is quantified by flow cytometry. A) Influence of liposome surface modification on cell association. Unmodified liposomes, or liposomes with ligands attached to lipid head groups (either biotin, fluorescein, or PEG2000) are incubated at 37 °C for the indicated time periods before cellular association is quantified. $n = 3$ per time point for each liposome type. B) Liposome shielding by scFvs. For the whole 24 h incubation period with fluoresceinated liposomes, an α-Flu scFv without or with a PAS tail of 11 PAS repeats is present at the indicated molar ratio relative to surface-accessible DSPE-Flu. The highest scFv:DSPE-Flu ratio corresponds to 15 µM α-Flu-PAS. $n = 3$ for each combination of scFv and scFv:DSPE-Flu ratio. C) Liposome deshielding by addition of free ligand. Fluoresceinated liposomes are shielded by incubation with PASylated α-Flu (molar ratio 4.5:1 relative to surface-accessible DSPE-Flu) and incubated with HeLa cells. After 2 h, fluorescein is added, and after 24 h, cellular association is quantified. $n = 3$ for each fluorescein:scFv ratio.

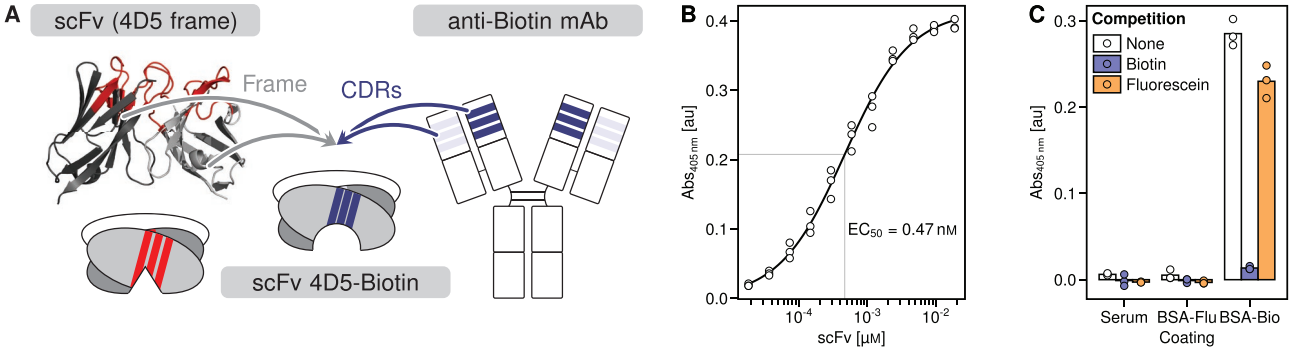

Figure 3. Design and characterization of a CDR-grafted biotin-binding scFv. A) Design of the CDR grafting. Framework regions are taken from the 4D5 V_H and V_L consensus sequences and combined with the CDR regions of a biotin-binding murine mAb. B) Binding curve of the grafted α-Biotin scFv. The binding capability of the grafted scFv to biotin-BSA is determined by ELISA. $n = 3$ for each scFv concentration. C) Specificity of the grafted α-Biotin scFv. Binding of the scFv to immobilized bovine serum, fluorescein-BSA, or biotin-BSA is measured by ELISA. For competition with the immobilized ligand, 500 μM free biotin or 500 μM free fluorescein is mixed with the scFv before addition to the coated wells. $n = 3$ for each combination of competition and coating.

to unmodified liposomes, $p > 0.9$, one-sided Dunnett test, $n = 3$ per group). In contrast, covalent PEGylation drastically reduced liposome association with cells as expected ($p < 0.001$ when AUCs of kinetic curves for PEGylated liposomes were compared to unmodified liposomes, one-sided Dunnett test, $n = 3$ per group).

Next, we tested whether we could shield fluoresceinated liposomes from cell association by non-covalent attachment of an scFv against fluorescein (α-Flu(H69A)), based on the FITC-E2 scFv[37] with an H69A mutation, facilitating production in *E. coli* at the expense of an increased K_D (from 0.75 to 8.9 nM).[38,39] To confer shielding properties on α-Flu(H69A), we fused 11 repeats of a 20 amino acid PAS sequence to its C terminus. α-Flu(H69A) and α-Flu(H69A)-PAS were produced in *E. coli* and purified by immobilized metal affinity chromatography (Figure S2A,B, Supporting Information).

To verify binding of the scFv to the liposomal surface, we measured the particle size of unshielded and shielded liposomes by dynamic light scattering (DLS; Figure S3, Supporting Information). Unshielded liposomes showed a Z average of (151 ± 2) nm, whereas this increased to (168 ± 7) nm for liposomes incubated with α-Flu(H69A), indicative of the increase in hydrodynamic radius by addition of the bulky PAS chains. This was in line with the previously reported hydrodynamic radius of a 200 amino acid (equivalent to 10 repeats) PAS peptide of approximately 4.9 nm.[35]

When the α-Flu(H69A) variants were allowed to bind to fluoresceinated liposomes and added to HeLa cells, α-Flu(H69A)-PAS dose-dependently reduced cellular association, whereas association remained high for α-Flu(H69A) without PAS (Figure 2B, Figure S4, Supporting Information). AUCs of the concentration curves differed significantly between both constructs when compared by *t*-test ($p < 0.001$, $n = 3$ per group), demonstrating that shielding of liposomes by attachment of a PASylated scFv is a feasible approach.

Next, we assessed the possibility of deshielding by addition of free ligand (Figures 1 and 2C and Figure S5, Supporting Information). To test this, we bound α-Flu(H69A)-PAS to fluoresceinated liposomes and incubated them with HeLa cells in the presence of different concentrations of free fluorescein. When association was quantified after 24 h, we found that fluorescein successfully deshielded the liposomes and reconstituted cellular association in a dose-dependent manner (Figure 2C and Figure S5, Supporting Information).

After we demonstrated (de)shielding with fluorescein, we tested whether we could adjust the system to respond to other trigger molecules by tailoring the small molecule-scFv affinity pair. For this purpose, we chose biotin as an alternative trigger molecule. In order to generate a biotin binder, we designed a humanized biotin-binding scFv from a biotin-binding murine monoclonal antibody (mAb).[40] We grafted the complementarity determining regions (CDRs) into the 4D5 scFv framework, a human consensus sequence originally applied to humanize the α-c-erbB2 mAb 4D5 (Herceptin)[41] (**Figure 3**A and Figure S6, Supporting Information). This antibody framework exhibits favorable folding and stability properties and has been successfully used for CDR grafting.[42,43] We produced the resulting α-Biotin scFv in *E. coli* and purified it by Protein L affinity chromatography (Figure S2C, Supporting Information). We measured the affinity of α-Biotin to biotinylated bovine serum albumin (BSA) by biolayer interferometry and determined its mean K_D at (66±21) nM (Figure S7A, Supporting Information). An ELISA experiment showed a half-maximal effective concentration (EC_{50}) of 0.47 nM (95% CI: 0.40–0.53 nM) (Figure 3B). Furthermore, competitive ELISAs revealed that free biotin competitively abolished binding of α-Biotin to BSA-Biotin, whereas fluorescein did not (Figure S7B, Supporting Information, and Figure 3C), confirming the specificity of α-Biotin to its ligand.

Next, we fused 11 PAS repeats to the C terminus of the biotin-binding scFv (α-Bio-PAS; Figure S2D, Supporting Information) and investigated its shielding capacity. Incubating biotinylated liposomes with α-Bio-PAS again reduced cellular association, and this effect was reversible by addition of free biotin (**Figure 4**A and Figure S8, Supporting Information). In contrast, α-Bio-PAS did not reduce cellular association of non-biotinylated liposomes, thus confirming specificity of the scFv binding (Figure S10A, Supporting Information).

Following these successful non-covalent shieldings of liposomes decorated with two distinct small molecules, we asked whether we could further extend our approach to another class of nanoparticle, and selected an adeno-associated viral

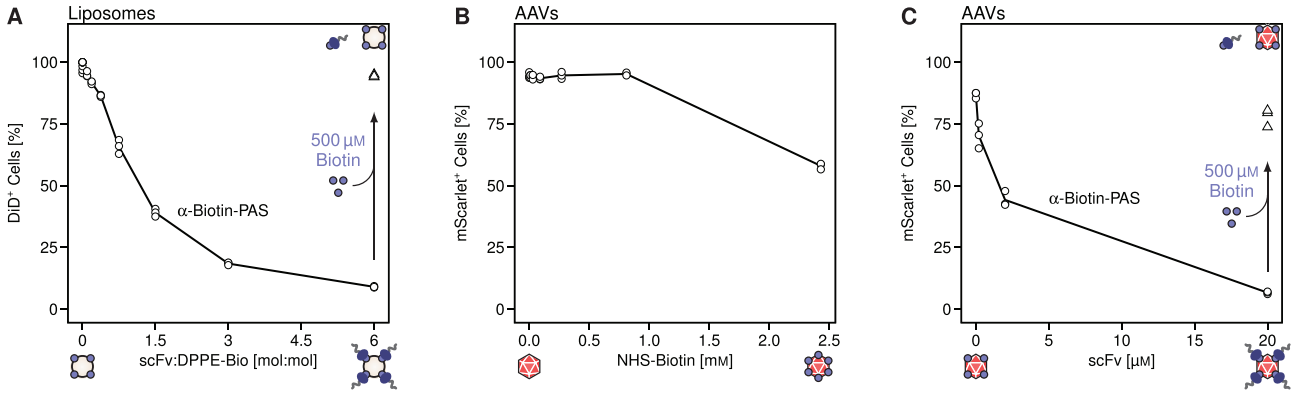

Figure 4. Shielding of biotin-modified liposomes or AAVs by PASylated scFvs prevents cellular association. A) Biotinylated DiD labeled liposomes are shielded (circles) with a PASylated (11 repeats) α-Biotin scFv (α-Biotin-PAS) and optionally deshielded (triangles) with 500 µM free biotin. After incubation with HeLa cells for 24 h, cell association is quantified by flow cytometry. The highest scFv:DPPE-Biotin ratio corresponds to 20 µM α-Biotin-PAS. For shielding, $n = 3$ for each scFv:DPPE-Bio ratio, except for the ratio of 0 ($n = 9$). For deshielding, $n = 3$. B) AAVs are surface-modified with NHS-biotin and the transduction efficiency is assessed by incubation with HEK-293T cells. After 24 h, mScarlet$^+$ cells are quantified by flow cytometry. $n = 3$ for each NHS-Biotin concentration. C) Biotinylated AAVs (modified with 0.45 mM NHS-biotin) are shielded/deshielded as the liposomes in (A). Transduction efficiency is assessed by incubation with HeLa cells. For shielding, $n = 3$ for each scFv concentration. For deshielding, $n = 3$.

vector (AAV) for this purpose. AAV virions are approximately 25 nm in diameter and are a leading tool for therapeutic gene delivery.[44] We functionalized the surface of AAVs carrying a transgene for the fluorescent protein mScarlet[45] with NHS-biotin, which reacts with primary amines, and tested the effect on transduction (Figure 4B). At high NHS-biotin concentrations (>2.4 mM), transduction was markedly impaired, indicating modification of AAV surface structures crucial for transduction, or interference with AAV structure and/or stability. Therefore, we, chose an NHS-biotin concentration of 0.45 mM for labeling, which was not detrimental to AAV functionality. Shielding with α-Bio-PAS reduced the fraction of mScarlet$^+$ transduced cells, whereas deshielding was accomplished after addition of free biotin (Figure 4C and Figure S9, Supporting Information). As for liposomes, addition of α-Bio-PAS to non-biotinylated liposomes did not decrease their transduction rate (Figure S10B, Supporting Information).

In summary, we could show that shielding of nanoparticles by non-covalent attachment of PASylated scFvs is feasible for different types of small molecules, and likewise for different types of nanoparticles.

2.2. Development of Fluorescein-Responsive Nanocomposite Hydrogels

Drawing inspiration from our previous experience with small molecule-responsive hydrogels[46] and incorporating our outlined strategy for nanoparticles, we set out to combine both approaches to develop controllable hydrogel-based depots for the triggered release of nanoparticles. First, we established the system with the example of fluorescein-responsive nanocomposite hydrogels for the release of liposomes and then demonstrated the versatility of the system by adapting it for the release of AAVs. The architecture of the gels consisted of non-covalently interacting 8-arm PEG-Fluorescein and 8-arm PEG-scFv conjugates. Entrapping fluorescein-labeled nanoparticles would allow to control their release and cellular interaction by the addition of free fluorescein, competitively displacing 8-arm PEG-Fluorescein and dissolving the hydrogel (**Figure 5**).

2.2.1. Generation of a Fluorescein-Binding scFv with Enhanced Stability

The synthesis reaction of fluorescein-responsive nanocomposite hydrogels based on the α-Flu scFv requires transiently high protein concentrations of approximately 60 to 70 mg mL^{-1} in order to meet the target concentration requirements of all reagents. Typically, such high protein concentrations are stabilized by addition of surfactants and excipients.[47] However, for hydrogel synthesis, reformulation of the scFv with additives is limited by the requirements for a defined reaction buffer.

As an alternative approach and encouraged by the successful construction of α-Biotin by grafting, we explored the possibility of increasing the stability of the anti-fluorescein scFv FITC-E2[37] by grafting its CDR regions to the 4D5 framework, resulting in α-Flu graft (Figure S11, Supporting Information).

We produced the grafted scFv in the cytosol of *E. coli* and used affinity chromatography for purification. Purification via a protein A agarose-based matrix yielded a higher purity compared to Ni^{2+}-NTA affinity chromatography (Figure S2E,F, Supporting Information).

To evaluate the fluorescein binding of the grafted scFv, we recorded a binding curve on immobilized, fluorescein-conjugated bovine serum albumin (BSA-Flu) by ELISA and obtained an EC_{50} of 1.5 nM (95% CI: 1.3–1.6 nM) (Figure S12A, Supporting Information). Calculation of the dissociation constant from association and dissociation rates measured by biolayer interferometry yielded a dissociation constant (K_D) of 2 nM (Figure S13A, Supporting Information). Because framework residues can also contribute to antigen binding,[48] we compared the K_D of α-Flu and α-Flu graft by fluorescence quenching of fluorescein at different scFv concentrations

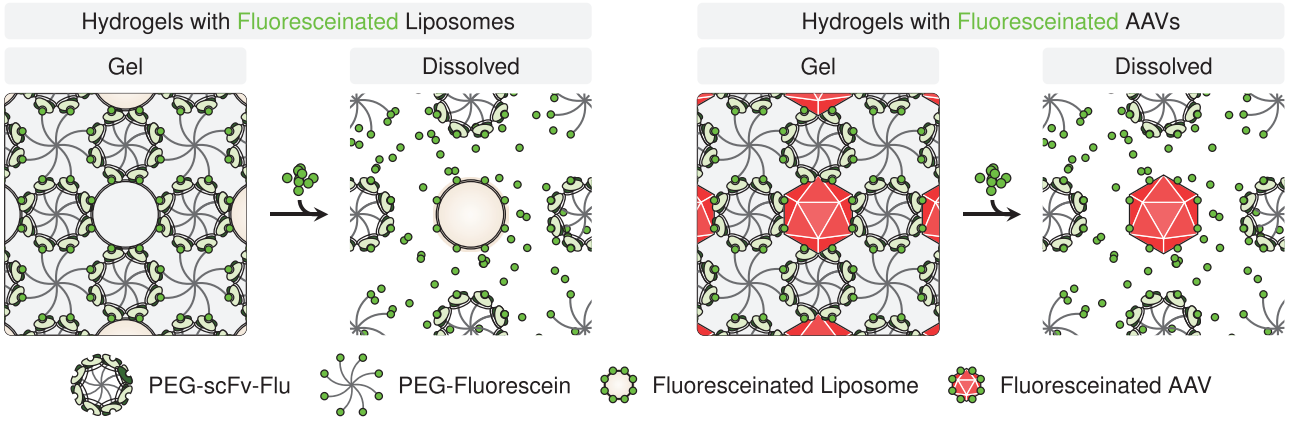

Figure 5. Active entrapment of liposomes or AAVs in fluorescein-responsive hydrogels. Multivalent interactions between 8-arm PEG fluorescein and 8-arm PEG-scFv conjugates result in the formation of a polymeric hydrogel network. Fluoresceinated liposomes or AAVs can actively participate in this interaction network and thus be immobilized. Addition of free fluorescein competes with the interactions stabilizing the hydrogel, resulting in its dissolution and release of its cargo. Illustrated components are not drawn to scale.

(Figure S13B, Supporting Information). Although we observed a slight decrease in affinity of α-Flu graft (K_D = 23.5 nM) in comparison to its ungrafted counterpart (K_D = 0.6 nM), the dissociation constant was still in the nanomolar range. Thus, the two methods were in good agreement within an order of magnitude and confirmed nanomolar affinity of the grafted scFv. As with α-Bio, we confirmed the specific binding of α-Flu graft to fluorescein by performing a competitive ELISA experiment. α-Flu graft only bound to immobilized BSA-Flu, but not to serum or BSA-Biotin. Only competition with free fluorescein abolished binding of the grafted scFv to the immobilized BSA-Flu (Figure S12B, Supporting Information).

Next, we characterized the grafted scFv with respect to its stability. We determined the thermal stability in comparison to the α-Flu(H69A) scFv. To this end, melting curves were determined by using SYPRO Orange, a dye that fluoresces upon binding to hydrophobic regions of denatured proteins. The grafted scFv showed a higher melting temperature (T_M = 70 °C) and thus a higher thermal stability than the CDR donor scFv (T_M = 60 °C) (Figure S12C, Supporting Information). Similarly, analysis of the tryptophan fluorescence in equilibrium denaturation experiments with guanidine hydrochloride revealed higher thermodynamic stability for the grafted scFv compared to the CDR donor scFv (Figure S12D, Supporting Information). These enhanced stability characteristics were also reflected in the binding capacity to BSA-Flu after prolonged storage. Whereas the ungrafted version lost approximately 50% activity after storage at 40 °C compared to storage at 4 °C for 3 weeks (as determined by ELISA), this deterioration was markedly diminished for the grafted variant even after 6 weeks (Figure S13C, Supporting Information).

2.2.2. Synthesis of Fluorescein-Responsive Hydrogels using the Grafted scFv

Following the successful graft of the FITC-E2 CDR regions into the stable 4D5 frame, we synthesized fluorescein-responsive hydrogels using this new variant.[46] To enable the chemoselective coupling to PEG-vinyl sulfone (PEG-VS), we fused a cysteine via a flexible serine-glycine linker to the C-terminus of the scFv (Figure S2G, Supporting Information). After letting the scFv bind to 8-arm PEG-fluorescein, we started the reaction of the 8-arm PEG-VS with the terminal cysteine by applying a one-pot thiol-ene click approach.[49] As a result, the PEG-fluorescein and PEG-scFv conjugates formed a stable hydrogel network. We qualitatively assessed different synthesis conditions and opted for performing all gel syntheses at a final scFv concentration of 30 mg mL^{-1} and a 1.5:1 molar ratio of PEG-VS:scFv (Figure S14, Supporting Information).

Afterward, we evaluated the mechanical properties and stimulus-responsiveness of the material (**Figure 6**). Amplitude sweep measurements at 1 Hz showed constant storage and loss moduli over a deformation range of ≈0.2% to 20% (Figure 6A). Subsequently, we performed rheology frequency-sweep experiments within the linear viscoelastic regime at a constant deformation of 0.5% (Figure 6B). In accordance with typical hydrogel properties, the storage modulus G′ exceeded the loss modulus G″ over the complete frequency range measured (0.01 to 1 Hz). At low frequencies, G′ decreased and G″ increased, indicating rearrangements of the physical crosslinks of the polymeric network typical for non-covalently crosslinked hydrogels.

Next, we quantified gel dissolution by measuring the amount of released protein in the supernatant. Without addition of free fluorescein, we observed a basal level, likely indicative of scFv molecules which had failed to undergo coupling to PEG-VS. Upon addition of increasing concentrations of fluorescein, the gels dissolved and their constituent protein was released in a dose-dependent fashion (Figure 6C). Addition of biotin instead of fluorescein did not result in protein release beyond the basal level, confirming the specific response of the hydrogels to the intended ligand (Figure S15, Supporting Information).

2.2.3. Active Entrapment of Liposomes or AAVs in Fluorescein-Responsive Hydrogels

The scale of typical pore sizes for hydrogels ranges from tens of nanometers[50] to tens of micrometers.[51,52] This is sufficiently

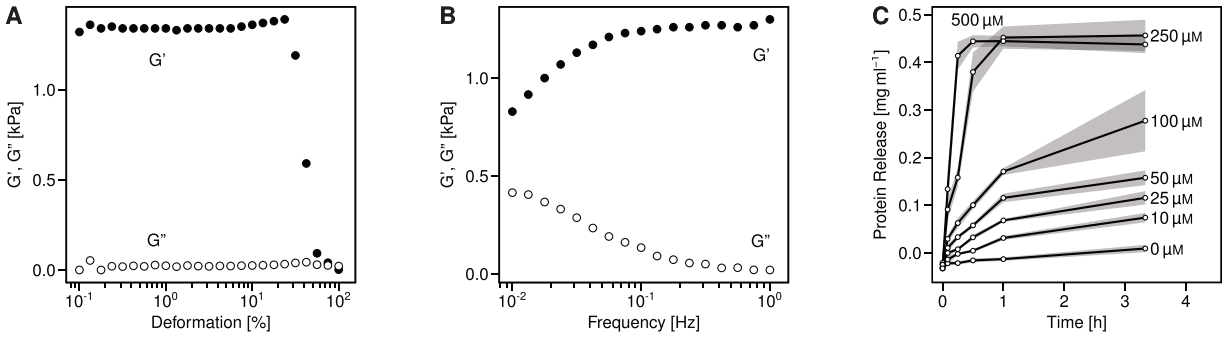

Figure 6. Synthesis and characterization of a fluorescein-responsive hydrogel. Hydrogels are synthesized using the grafted α-Flu scFv. A,B) Mechanical characterization. Hydrogel discs are pre-swollen in phosphate buffered saline (PBS). The storage (G′) and loss (G″) moduli are determined by small amplitude oscillatory shear rheology A) over a deformation range of 0.1 to 100% at 1 Hz, or B) over a frequency range of 0.01 to 1 Hz at a constant deformation of 0.5%. C) Fluorescein-triggered dissolution. Hydrogels are incubated in PBS with the indicated concentrations of free fluorescein. Dissolution is monitored by determining the released scFv in the supernatant with the bicinchoninic acid (BCA) assay. $n = 6$ gels per dissolution time course, symbols and lines mark the mean and ribbons show standard deviation.

small to passively entrap large complexes such as antigen-alum complexes,[46] which form micrometer-sized aggregates.[53] However, small molecules cannot be stably entrapped in this fashion because they would diffuse out of the hydrogel into the surrounding medium. This is apparent even for small proteins, which are released from porous hydrogels within a few hours.[54] Here, we investigated whether we could achieve liposome and AAV entrapment in fluorescein-responsive hydrogels.

When we added DiD labeled liposomes to the hydrogel synthesis reaction, we found that they did not remain stably associated, but passively diffused out of the gels even preceding addition of fluorescein to induce gel dissolution (**Figure 7**A and Figure S16A, Supporting Information). However, when we made fluorescein available on the surface of the liposomes by post-insertion[55] of DSPE-Flu (Figure S17, Supporting Information) and thus allowed the liposomes to be a structural component of the hydrogel framework, this leakiness was almost completely abolished, and release could still be triggered by free fluorescein (Figure 7A and Figure S16A, Supporting Information). The gels also tightly retained their cargo in synthetic body fluid (SBF, a buffer solution with ion concentrations closely mimicking acellular blood plasma[56]) and in complete cell culture medium with fetal calf serum (FCS). Fluorescein-triggered complete dissolution in these buffers was possible for at least 10 days after gel synthesis, although dissolution kinetics reduced slightly over time (Figure S16B, Supporting Information).

Next, we tested whether liposomes released from the gels would associate with cells. We prepared gels with different ratios of DSPE-Flu, placed the gels on HeLa cells, and measured liposome association after 24 h (Figure 7B and Figures S16C and S18, Supporting Information). Without a dissolution trigger, (49.9 ± 1.5)% of cells became DiD^+ upon incubation with hydrogels containing liposomes with 0.1 mol% DSPE-Flu, whereas this leakiness was reduced to (4.5 ± 2.6)% and (0.4 ± 0.2)% for liposomes with 0.25 mol% or 1.0 mol% DSPE-Flu, respectively. Dissolving the gels with 500 µM fluorescein increased the fraction of cells associated with liposomes to (95.4 ± 1.2)% for liposomes with 0.1 mol% and to (94.4 ± 0.3)% for liposomes with 0.25 mol% DSPE-Flu. Conversely, this increase only reached (52.8 ± 1.4)% for liposomes with 1 mol% DSPE-Flu. We hypothesize that this lower liposome-cell association was a consequence of residual PEG-scFv still attached to the liposomal surface, which acted as a shielding layer.

After establishing the gel system with empty liposomes, we extended it to cargo-loaded liposomes. We synthesized DiD labeled liposomes and performed remote-loading of doxorubicin via an ammonium sulfate gradient.[57] However, dry lipid cakes containing DSPE-Flu could not be hydrated in ammonium sulfate without the formation of aggregates, and the addition of doxorubicin to solutions containing DSPE-Flu likewise induced aggregation. To circumvent this issue, doxorubicin was first loaded into liposomes before addition of DSPE-Flu and subsequent post-insertion. This allowed encapsulation of doxorubicin into fluorescein-modified liposomes (Figure S19A, Supporting Information), but leakage was increased compared to unmodified liposomes (Figure S19B, Supporting Information).

The doxorubicin charged or empty liposomes were modified with 1 mol% DSPE-Flu by post-insertion and then used to synthesize hydrogels. After 24 h incubation with HeLa cells, we measured cell proliferation via WST-1 assay (Figure S20, Supporting Information). To avoid possible influences of physical contacts between cells and the gel matrix on the proliferation readout, the gels were placed in the upper compartment of a transwell insert without direct contact with the cell layer. We observed baseline toxicity of doxorubicin-charged hydrogels. Given that we observed negligible association between uncharged liposomes and cells without gel dissolution (Figure 7B), we speculated this was due to leakage of highly potent free doxorubicin from the charged liposomes, and not due to leakage of liposomes from the gel. Measurements of DiD and doxorubicin fluorescence in the supernatant supported this notion and revealed some leakage of doxorubicin, but not of liposomes (Figure S21, Supporting Information). Nevertheless, release of doxorubicin-loaded liposomes by addition of fluorescein significantly decreased cell viability ($p < 0.001$, t-test between conditions with and without addition of fluorescein, $n = 8$ per group), and the reduction in viability (to (49.8 ± 3.9)%) was in agreement with the previously observed fraction of cells

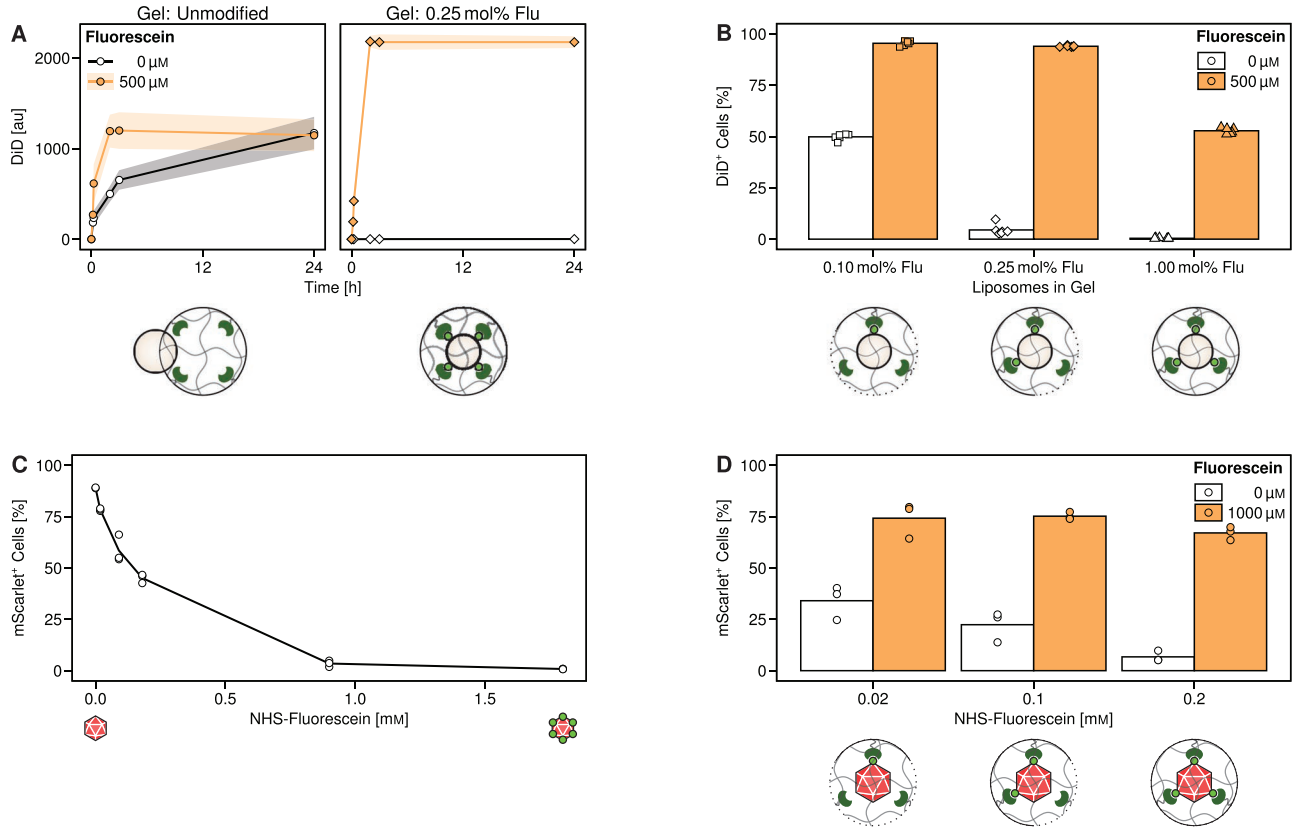

Figure 7. Entrapment of liposomes or AAVs in hydrogels and their fluorescein-dependent release. A) Fluorescein-dependent release kinetics of hydrogels with incorporated DiD labeled liposomes without (left panel) or with 0.25 mol% (right panel) surface-exposed fluorescein. Hydrogels are incubated in PBS with or without fluorescein and liposomal release is quantified by measuring DiD fluorescence in the supernatant. The difference in absolute values is due to loss of unmodified liposomes during wash steps (Figure S16A, Supporting Information). $n = 6$ gels for each dissolution time course, symbols mark the mean and ribbons show standard deviation. B) Availability of hydrogel-entrapped liposomes to cells. Hydrogels loaded with liposomes with the indicated amounts of surface-exposed fluorescein are placed on HeLa cells in complete medium with or without fluorescein. After 24 h, association of liposomes with cells is quantified by flow cytometry. $n = 6$ gels for each condition. C) AAVs carrying the mScarlet transgene are surface-modified with different concentrations of NHS-fluorescein. Transduction of HEK-293T cells is measured by flow cytometry after 24 h. $n = 3$ for each concentration of NHS-fluorescein. D) AAVs carrying the mScarlet transgene are surface-modified with different concentrations of NHS-fluorescein and concentrated via dialysis. The AAVs are entrapped in fluorescein-responsive hydrogels, which are placed on HeLa cells and incubated with or without fluorescein. After 24 h, transduction is quantified by flow cytometry. $n = 3$ gels for each condition.

associating with uncharged liposomes (52.8 ± 1.4%). In contrast, releasing empty liposomes did not significantly impact viability ($p > 0.3$, t-test between conditions with and without addition of fluorescein, $n = 8$ per group; Bonferroni corrected with prior t-test) (Figure S20, Supporting Information).

We next tested whether we could generalize our approach of releasing liposomes from a fluorescein-responsive hydrogel to another type of nanoparticle. As our experiments had demonstrated that scFvs could be used to confer shielding properties on AAVs, we chose this same type of AAV for our subsequent experiments.

We first verified if we could label AAV capsids with NHS-fluorescein and observed a dose-dependent decrease in transduction efficiency upon incubation with HEK-293T cells, compared to unmodified AAV (Figure 7C). For subsequent experiments, we chose NHS-fluorescein concentrations that did not abolish functionality of AAV (≤0.2 mM). We concentrated the fluoresceinated AAVs by ultrafiltration and prepared fluorescein-responsive hydrogels. When we placed these gels on HeLa cells, we saw a fluorescein dose-dependent increase in transduced mScarlet$^+$ cells, indicative of dissolution of the gels and release of AAVs (Figure S22, Supporting Information). However, incorporation of AAV into hydrogels was challenging, because ultrafiltration led to loss of a large fraction of input AAV. Consequently, transduction of only (18.7 ± 2.6)% of cells was achieved.

To address this limitation, we explored a more gentle approach for concentration: After coupling of AAVs with NHS-fluorescein, we placed them in a dialysis cassette and performed volume reduction by submersion in a buffer containing 40% (w/v) PEG-20. This allowed us to entrap a higher number of AAV particles in the hydrogels, resulting in high transduction ratios after dissolution of the gels (Figure 7D and Figure S23, Supporting Information). Of note, the transduction of HeLa cells by AAV released from the hydrogel depots was higher compared to the transduction of HEK-293T cells by

"free" AAV labeled with the same concentration of NHS-fluorescein in Figure 7C. Since the AAV-2 transduction efficiency of both cell lines is comparable,[58,59] the difference is likely due to the higher concentration of AAV for gel synthesis and thus the entrapment and release of higher numbers of AAV particles per cell culture well. Similar to our observations for liposome-loaded gels, functionalization of AAV with higher amounts of fluorescein decreased leakiness, but also slightly impaired transduction after dissolution of the gels. This is likely a combination of the reduced AAV transduction efficiency after labeling and residual PEGylated scFvs acting as a shielding layer.

3. Conclusions

In this study, we demonstrated how the reversible interactions between scFvs and their ligands can be exploited for rational and modular nanoparticle design. By surface-functionalization of nanoparticles with scFv ligands, we upgraded the particles to allow attachment of functionally modified scFvs. Instead of pursuing further modification to the nanoparticles to accommodate different use cases, we customized the scFv component. Specifically, we showed shielding of nanoparticles from cellular binding by non-covalent attachment of a shielding polymer, and the active incorporation of nanoparticles into fluorescein-responsive hydrogels. We demonstrated the versatility of this approach by using the unrelated small molecules fluorescein and biotin, and two distinct types of nanoparticles, liposomes, and AAVs. Due to the reversibility of the exploited scFv-ligand interactions, we were able to detach the shielding layer or dissolve the hydrogels by the addition of a free trigger molecule, which was also used for the preceding functionalization of the nanoparticles. This form of exogenous stimulus-responsiveness provides a facile method for the scheduled activation of shielded nanoparticles, and for the dissolution of nanocomposite hydrogels.

Future efforts should be directed towards elucidating open questions regarding application of the prototypic systems presented herein for in vivo settings. For instance, the dose and the bioavailability of orally ingested or injected trigger molecules must be both tolerable and sufficient to induce release. Existing data for fluorescein suggests that this would be the case: In pigs, intravenous administration of 15 mg kg^{-1} fluorescein raised concentrations of fluorescein to approximately 10–20 g L^{-1} (30–60 μM) in a variety of tissues.[60] In a human patient, administration of an even higher dose (40 mg kg^{-1}) for delineation of a glioma during surgical resection was well tolerated,[61] although typically, lower doses (5–20 mg kg^{-1})[62,63] are used for this application. Importantly, there is direct evidence of the feasibility of administering high doses in mice: Four oral doses of ≈1000 mg kg^{-1}, given over three days, led to dissolution of a subcutaneously implanted fluorescein-responsive hydrogel.[46]

Likewise, the toxicity of biotin is low[24] and its LD_{50} value in rodents was >10 000 mg kg^{-1} (oral) or >1000 mg kg^{-1} (intravenous).[64] In rats, oral uptake of 1000 mg kg^{-1} day^{-1} over 36 weeks resulted in a peak plasma concentration of ≈10 μg mL^{-1} (40 μM).[64] On a functional level, it was shown that intraperitoneal administration of 100 mg kg^{-1} biotin could trigger a biotin-responsive gene switch in mice.[65]

Taken together, these data suggest that sufficient concentrations of fluorescein or biotin are attainable for triggering delivery systems responsive to these small molecules.

In summary, we showed that our system allows triggered delivery of small-molecule cargo in liposomes and of adeno-associated viral vectors in vitro.

4. Experimental Section

Plasmids and Protein Constructs: Plasmids and protein constructs used in this study are summarized in Table S1, Supporting Information, with DNA sequences, expression, and purification conditions. Buffer exchange of purified proteins into the respective assay buffer (as specified in the relevant experimental sections) was carried out by dialysis with SnakeSkin dialysis tubing (3.5 kDa MWCO, Thermo Fisher Scientific, #11532541). Proteins were concentrated by ultrafiltration in spin concentrators with a 10 kDa MWCO PES membrane (Sartorius, #VS15T02). Concentration of proteins in solution was determined with a NanoDrop 2000 spectrophotometer (Thermo Fisher Scientific), using theoretical extinction coefficients calculated by SnapGene (GSL Biotech).

Protein Production and Purification: For a summary of the expression and purification procedures used for different proteins, see Table S1, Supporting Information. After expression in *E. coli*, cells were harvested at 6000 g for 10 min and resuspended in 35 mL lysis buffer (50 mM NaH_2PO_4, 300 mM NaCl, 10 mM imidazole, pH 8.0) per 1 L culture. The cells were disrupted using a French press at 1000 bar and 4 °C. Insoluble material was removed by centrifugation at 30 000 g for 1 h at 4 °C. Optionally, proteins were precipitated in solutions of $(NH_4)_2SO_4$ for 1 h at 4 °C. The precipitate was pelleted by centrifugation at 30 000 g for 1 h at 4 °C and resuspended in lysis buffer. The resuspended precipitates or cleared lysates were purified by affinity chromatography with Ni-NTA agarose (Qiagen, #30450) or Capto L agarose (Cytiva, #17-5478-06) in manually packed gravity flow columns (bed volume 2 mL), or with a prepacked column of protein A agarose (GE Healthcare, #17-0403-01) on an Äkta Express fast protein liquid chromatography system (FPLC, GE Healthcare). Following sample loading, columns were washed with 20 column volumes of wash buffer and elution was performed with 6 column volumes of elution buffer.

For purification with Ni-NTA agarose, wash buffer was 50 mM NaH_2PO_4, 300 mM NaCl, 20 mM imidazole, pH 8.0, and elution buffer was 50 mM NaH_2PO_4, 300 mM NaCl, 250 mM imidazole, pH 8.0.

For purification with protein A or Capto L agarose, wash buffer was PBS (2.7 mM KCl, 1.5 mM KH_2PO_4, 8.1 mM Na_2HPO_4, 137 mM NaCl), and elution buffer was 0.1 M glycine, pH 3.0. After elution, the pH was neutralized by the addition of 1 column volume 1 M Tris-HCl (pH 8.0).

Purity was evaluated by sodium dodecyl sulfate (SDS)-polyacrylamide gel electrophoresis (SDS-PAGE) and subsequent Coomassie staining.

Preparation of Liposomes: Liposomes were prepared using the thin-film hydration method. Unmodified liposomes were prepared by mixing HSPC (Lipoid, #525600) and cholesterol (Sigma-Aldrich, #C3045) at a molar ratio of 60:40 in a 100 mL round bottom flask. Additional lipids were added at the expense of HSPC and cholesterol proportionally. The lipophilic tracer DiD (Thermo Fisher Scientific, #D7757) was included at a final concentration of 0.08 mol% for shielding experiments, or of 0.5 mol% for hydrogel experiments. For shielding experiments, final concentrations of 5 mol% DSPE-PEG2000 (Lipoid, #588200), 4 mol% DSPE-Flu or 4 mol% DPPE-Biotin (Avanti, #870285P), respectively, were also added. Chloroform was removed by rotary evaporation. The dry lipid film was hydrated in PBS at 70 °C with intermittent vortexing to achieve a final total lipid concentration of approximately 20 mM. The resulting heterogeneous liposome suspension was extruded using an Avanti Mini Extruder (Avanti, #610023) at 70 °C, with 23 passages through a 200 nm membrane (Cytiva, #10417004) and 12 passages through a 100 nm membrane (Cytiva, #800309). If required for downstream applications, liposomes were concentrated

by ultrafiltration in spin concentrators with a 100 kDa MWCO RC membrane (Merck, #UFC810024). The lipid concentration of liposomes was determined by comparing the DiD fluorescence of the sample with a reference standard.

Fluorescence Measurements of Liposomes: All fluorescence measurements of DiD were made with an Infinite M200 pro microplate reader (Tecan) at 640 nm/680 nm (Ex/Em). Doxorubicin fluorescence was measured at 490 nm/580 nm (Ex/Em). If not specified otherwise, liposomes were lysed in PBS with 1% (v/v) Triton X-100 (Roth, #3051.4) at 70 °C for 15 min before measuring.

Post-Insertion and Doxorubicin Loading of Liposomes: For incorporation into hydrogels, liposomes were modified with DSPE-Flu by post-insertion, because DSPE-Flu was incompatible with hydration in 250 mM $(NH_4)_2SO_4$ required for doxorubicin loading.

DSPE-Flu was dried from chloroform and micellularly solubilized by hydration in PBS at 70 °C to a concentration of 3.84 mM. Micelles were added to liposomes in PBS (10 to 20 mM in 1 mL) to achieve the desired final mol% content of DSPE-Flu, assuming a post-insertion efficiency of 86% (Figure S17, Supporting Information). The mixture was incubated for 1 h at 70 °C, and unincorporated micelles were removed by gravity flow over 10 mL of a Sepharose CL-2B matrix (Cytiva, #17-0140-01).

For doxorubicin loading, liposomes were hydrated in 250 mM $(NH_4)_2SO_4$. After extrusion, a gradient was established by passage over a Sepharose CL-2B column equilibrated with PBS. Doxorubicin was added at a molar ratio of 1:3.5 (drug:lipid). Doxorubicin is carcinogenic and cardiotoxic, and must be handled with the necessary safety precautions. Loading was allowed to proceed for 30–45 min at 70 °C before performing post-insertion and removing unincorporated micelles and doxorubicin, as described above.

Cell Culture: HeLa cells and HEK-293T were cultured in DMEM (PAN Biotech, #P04-03550), supplemented with 10% (v/v) FCS (PAN Biotech, #P30-3602) and 1% (v/v) penicillin-streptomycin (PAN Biotech, #P06-07100) in a humidified atmosphere with 5% CO_2. If not specified otherwise, cells were seeded at a density of 5000 cells per well in a 96 well cell culture plate and assays were performed in a culture volume of 100 µL.

Flow Cytometry: The culture supernatant was removed, and cells were washed once with PBS before detachment with 50 µL Trypsin (PAN Biotech, #P10-023500). After incubation for 5 min at 37 °C, 50 µL FACS Buffer (PBS, 4% (v/v) FCS, 2 mM EDTA) were added, cells were centrifuged at 300 g for 5 min and resuspended in 200 µL FACS Buffer. Data were acquired on a Gallios flow cytometer (Beckmann Coulter) or an Attune NxT flow cytometer (Thermo Fisher Scientific) and analyzed with openCyto.[66] Association of liposomes with cells was quantified by gating for DiD^+ cells, whereas transduction by AAVs was quantified by gating for $mScarlet^+$ cells. Gates were constructed based on the untreated control after excluding debris and aggregates. Representative scatter plots illustrating the gating strategies are available in the Supporting Information.

Determination of Association Kinetics between Liposomes and Cells: Cells were seeded and allowed to adhere for 24 h. The culture medium was replaced by medium containing liposomes at phospholipid concentrations of 100 µM (167 µM total lipid) either 8, 4, or 2 h before analysis. Association of liposomes with cells was quantified via flow cytometry after incubation for the respective time spans at 37 °C.

Liposome Shielding and Deshielding: All proteins used for shielding were dialyzed against His Buffer (10 mM L-Histidine (Roth, #1696.2), 140 mM NaCl, pH 7.4) and concentrated to 5 to 10 mg mL^{-1}. Liposomes and shielding proteins were mixed in culture medium to achieve a final phospholipid concentration of 100 µM (167 µM total lipid) with varying molar ratios of protein to liposome-bound and surface-exposed ligand. For liposomes hydrated with DSPE-Flu or DPPE-Biotin, 50% of the incorporated ligand were assumed to be surface-exposed, with the other 50% facing the aqueous core of the liposome, rendering them inaccessible to proteins. For liposomes undergoing post-insertion, 100% of the ligand was assumed to be accessible. 100 µL of the liposome-protein mixture was added to cells 24 h after seeding and incubated for another 24 h before determination of liposome association with cells by flow cytometry. For deshielding experiments, free ligand was added 2 h after the start of the incubation period.

Viability Assay: Cells were seeded in MultiScreen 96 well receiver plates (Merck, #MATRNPS50), previously coated with 100 µg mL^{-1} rat collagen I (Thermo Fisher Scientific, #A1048301) in PBS for 3 h at room temperature. After 24 h, the culture supernatant was replaced with 300 µL fresh medium. A MultiScreen MESH Filter Plate (Merck, #MANMN2010) was placed on the plate, and 10 µL hydrogels were placed in the upper compartment before adding another 100 µL of medium. After 24 h, the culture supernatant was removed and replaced by 100 µL complete medium supplemented with a WST-1 based cell proliferation reagent (1:10 dilution; Sigma-Aldrich, #11644807001). The conversion of the tetrazolium salt WST-1 to a soluble formazan correlates with the metabolic activity of the cells and was monitored by measuring the increase in absorbance at 440 nm at 37 °C for 1 h.

Production and Purification of AAV-2 Vector: AAV-2 vector was produced using the adenovirus helper-free production system[67] and plasmids pHJW163 (AAV-2 rep-cap plasmid), pCMVmScarlet (vector plasmid; kind gift from Dirk Grimm), and pHelper (Cell Biolabs, #VPK-402) in a 1:1:2 molar ratio. Briefly, 5×10^6 HEK-293T cells (DSMZ, #ACC 635) were seeded in 15 cm cell culture dishes. After 48 h, the cells were transfected with 62.45 µg plasmid DNA, 206 µg polyethylene imine (25 000 Da), and 3 mL OptiMEM (Thermo Fisher Scientific, #22600-134). 5 h post-transfection, the cell culture medium was replaced with fresh medium. 72 h post-transfection, the cells were harvested by scraping them from the culture dishes and centrifuged at 400 g for 15 min. AAV-2 vector was purified from both the supernatant and cell pellet.

AAV-2 vector in the supernatant was precipitated by the addition of 25 mL PEG-8000 solution (40% (w/v), 0.41 M NaCl) per 100 mL of cell culture supernatant and stirring for 1 h at 4 °C, followed by an additional incubation step overnight without stirring. Precipitated vector was pelleted by centrifugation at 2818 g for 15 min at 4 °C and then resuspended in PBS. AAV-2 vector in the cells was released by washing the cell pellet first in PBS and then in virus lysis solution (50 mM Tris-HCl, 150 mM NaCl, pH 8.5), followed by five freeze-thaw cycles.

Vector preparations derived from the supernatant and cell pellet were combined and treated with benzonase (50 U mL^{-1}, Merck, #344 70664-3) at 37 °C for 1 h. Cellular debris was removed by three rounds of centrifugation at 4000 g for 15 min. The cleared AAV-2 vector sample was filtered through a 0.45 µm filter (Fisher Scientific, #15191499) and applied to a HiTrap AVB Sepharose column (Cytiva, #28411211) equilibrated with AVB wash buffer (20 mM Tris, 0.5 M NaCl, pH 8.0) using an Äkta Express FPLC system (GE Healthcare). After washing with 10 column volumes wash buffer, AAV-2 was eluted with 0.1 M sodium acetate, 0.5 M NaCl, pH 2.5, and the pH was neutralized with 1 M Tris, pH 8.7. Purified AAV-2 vector was dialyzed against 50 mM HEPES, 150 mM NaCl, and 2 mM $MgCl_2$, pH 7.4, supplemented with 10% (v/v) glycerol, and stored at −80 °C until use. Capsid titers were determined as described elsewhere.[68]

Synthesis of Biotin-rAAV-2 and Fluorescein-rAAV-2 Conjugates: NHS-biotin (Cayman Chemical, #Cay13315-100) and NHS-fluorescein (Thermo Fisher Scientific, #46410) were dissolved in *N*,*N*-Dimethylformamid (anhydrous; Sigma-Aldrich, #227056) to a final concentration of 20 mM. For the conjugation of biotin or fluorescein to rAAV-2, 1.12×10^{11} viral particles (VP) mL^{-1} were mixed with the indicated concentrations of NHS-biotin stock or NHS-fluorescein stock, respectively, and allowed to react for 3 h at room temperature. Unreacted NHS-biotin or NHS-fluorescein was removed by dialysis against 20 mM HEPES, 150 mM NaCl, 2 mM EDTA, 2 mM $MgCl_2$, 0.001% (v/v) Pluronic F-68, pH 7.4.

AAV Shielding and Deshielding: AAV shielding experiments were performed similarly to liposome shielding experiments, but 0.75 µL (8.4×10^7 VP) of biotinylated AAVs were used for transduction of each well. AAVs used for shielding experiments were biotinylated with 0.45 mM of NHS-biotin stock.

Determination of Particle Size by DLS: Liposomes (100 µM total lipid) were incubated with PASylated proteins (10 µM) in His buffer for 1 h at 37 °C. DLS was performed in a Zetasizer Nano S90 (Malvern) at 25 °C and a scattering angle of 90°.

Evaluation of Protein Stability: The thermal stability of scFvs was determined using the fluorescent SYPRO Orange dye (Thermo Fisher

Scientific, #S6650) in a real-time PCR thermal cycler (qTower 2.0/2.2, Analytik Jena). The scFv samples were prepared in PBS (4 µM final concentration) containing SYPRO Orange dye (diluted 1:1250). Thermal melting curves were recorded at 565 nm/606 nm (Ex/Em) by raising the temperature from 25 to 90 °C at intervals of 1 °C every 30 s.

Thermodynamic stabilities were determined by incubating the scFv constructs (0.8 µM of the grafted construct and 0.6 µM of the CDR donor scFv FITC-E2 (H69A) construct) with different concentrations of guanidine hydrochloride in 50 mM Tris-HCl, 100 mM NaCl, pH 7.2 at room temperature overnight. Tryptophan fluorescence maxima were determined by recording the emission intensities from 300 to 360 nm at an excitation wavelength of 280 nm in an Infinite M200 pro microplate reader (Tecan). Data analysis was conducted as described elsewhere.[69]

ELISA: ELISA was performed by coating 96 well plates (Corning, #CORN3590) with fluorescein- or biotin-conjugated BSA (Roth, #T844.3; 1 µg in 100 µL PBS per well) overnight at room temperature. Wells were washed 3× with 300 µL wash buffer (PBS, supplemented with 0.05% (v/v) Tween-20) and blocked with 300 µL blocking buffer (1% (w/v) BSA in PBS) for 1 h at room temperature. After washing 3× with wash buffer, the wells were incubated with scFv samples (diluted in blocking buffer) for 1 h at room temperature. Wells were washed 3× with wash buffer, probed with 100 µL anti-His antibody (1:1000 in blocking buffer; Merck, #70796) for 1 h at room temperature, washed again and incubated with anti-mouse IgG-HRP (1:2500 in blocking buffer; Santa Cruz, #sc-2005) for 1 h at room temperature. After washing 3× with wash buffer, the HRP activity was monitored by adding 100 µL 2,2′-azino-bis(3-ethylbenzothiazoline-6-sulphonic acid) (ABTS, Sigma-Aldrich, #A1888; 0.5 mM in 50 mM citric acid, pH 4.0, supplemented with 0.05% (v/v) H_2O_2) and measuring the absorbance at 405 nm in a microplate spectrophotometer. For competitive ELISA assays, the competing ligand was mixed with the scFv 30 min prior to addition to the coated wells.

Determination of Dissociation Constant by Fluorescence Titration: Dissociation constants of scFv-fluorescein affinity pairs were determined by fluorescence titrations.[38] Fluorescence spectra from 500 to 550 nm (440 nm excitation) were measured using dilutions of scFv (0 µM to 3 µM) and 0.1 µM fluorescein at room temperature. The fluorescence intensity maxima (at 516 nm) were plotted against the scFv concentrations and K_D values were calculated as described elsewhere.[38]

Biolayer Interferometry: Association and dissociation rates were determined by biolayer interferometry using the Octet RED96 System (Pall ForteBio LLC) at an assay temperature of 30 °C. Aminopropylsilane (APS) biosensors were loaded with unconjugated BSA, or with fluorescein- or biotin-conjugated BSA (10 µg mL^{-1} in PBS). After equilibration with assay buffer (PBS supplemented with 1% (w/v) BSA), the association of dilutions of scFv was monitored, followed by their dissociation in assay buffer. Control biosensors loaded with unconjugated BSA, which showed no association with the highest applied scFv concentrations, were used as reference for the biotin-binding scFv and were subtracted from the data. Similarly, the highest applied fluorescein-scFv showed no unspecific association to BSA. The background signal of biosensors loaded with fluorescein-BSA was subtracted from the data. Association and dissociation curves were locally fitted according to a 1:1 bimolecular interaction model (full fit for the α-Flu scFv, partial fit for the α-Biotin scFv).

Hydrogel Synthesis: For the synthesis of hydrogels, purified scFvs were dialyzed against hydrogel buffer (20 mM HEPES, 500 mM NaCl, pH 8.0). Typical 5 µL hydrogels were prepared by combining 150 µg scFv with tris-(2-carboxyethyl)-phosphine (TCEP; Roth, #HN95.1; TCEP:scFv = 0.7; mol:mol) and adding 0.5 µL 1 M triethanolamine (Roth, #6300.1), pH 8.0, and 8-arm PEG-fluorescein (scFv:fluorescein = *1:1.2;* mol:mol).[46] After incubation at room temperature for 30 min, 8-arm PEG-VS (40 kDa; NOF Europe, #Sunbright HGEOS-400VS) was added at a molar ratio of 1:1.5 (scFv:VS).

For the synthesis of liposome-loaded hydrogels, liposomes were added to the reaction mixture to a final concentration of 10 mM. For liposomes containing fluorescein, the total amount of fluorescein in the reaction was kept constant by reducing the amount of 8-arm PEG-fluorescein proportionally.

For the synthesis of rAAV-2 depots, purified rAAV-2 was concentrated by dialysis against 40% (w/v) PEG-20 (Sigma-Aldrich, #81300), 0.001% (v/v) Pluronic F-68, 20 mM HEPES, 500 mM NaCl, pH 8.0 for 40 min at room temperature using Slide-A-Lyzer dialysis cassettes (10 kDa MWCO, Thermo Fisher Scientific, #66383). The concentrated rAAV-2 (5×10^8 VP per 5 µL gel) was mixed with the hydrogel mixture prior to the addition of 8-arm PEG-VS.

The reactions were pipetted onto siliconized (Sigmacote; Sigma-Aldrich, #SL2) glass slides and incubated at room temperature in a humidified atmosphere for 20 h. After polymerization, the hydrogels were transferred into 300 µL hydrogel buffer supplemented with 100 mM monoethanolamine (Sigma-Aldrich, #E0135) to quench unreacted groups for 2 h at room temperature. Subsequently, gels were washed 3× in the buffer used for downstream applications for 1 h at room temperature.

Mechanical Hydrogel Characterization: 50 µL hydrogels were prepared between siliconized glass slides (1 mm height) and incubated in PBS at room temperature overnight. Small amplitude oscillatory shear measurements were conducted using an MCR301 rheometer (Anton Paar) with parallel plates at 25 °C. The hydrogels were placed between the plates (upper plate: 8 mm diameter, PP08, Anton Paar) and the gap was adjusted to 0.3 mm.

Statistics: Sample sizes in cell culture experiments reflect independently treated wells of a culture plate.

Statistical testing of liposome association was performed by calculating the AUC for each time course (for Figure 2A) or each concentration series (Figure 2B). AUCs were determined with the trapezoidal rule. For this purpose, individual data points were arbitrarily assigned to a replicate number for each x value, and AUCs were calculated for the curves formed by these replicates.

Data ranges in the text reflect mean ± standard deviation, except for EC_{50} and IC_{50} values.

To determine absolute EC_{50} and IC_{50} values by ELISA, the *drc* package[70] for R 4.1.1[71] was used. The indicated errors represent 95% confidence intervals.

Supporting Information

Supporting Information is available from the Wiley Online Library or from the author.

Acknowledgements

The authors are grateful for outstanding technical support by Denise Gaspar, Elke Wehinger-Welte, Susanne Knall, and Frauke Bartels-Burgahn. The authors would also like to thank Dirk Grimm (Heidelberg University, Germany) for providing the plasmid pCMVmScarlet. This work was supported by the Deutsche Forschungsgemeinschaft (DFG, German Research Foundation) under Germany's Excellence Strategy CIBSS – EXC-2189 – Project ID: 390939984 and under the Excellence Initiative of the German Federal and State Governments – EXC-294 and GSC-4, and in part by the Ministry for Science, Research and Arts of the State of Baden-Württemberg. This work was supported by the EU Framework Programme for Research and Innovation Horizon 2020 with a Grant from the European Research Council (ERC) Action No. 755369-DeShield.

Open access funding enabled and organized by Projekt DEAL.

Conflict of Interest

The University of Freiburg has filed a patent application of which B.R., M.D.Z., and W.W. are inventors. The remaining authors have no competing interests to declare.

Data Availability Statement

Research data are not shared.

Keywords

adeno-associated viruses, complementarity determining region grafting, hydrogels, nanoparticles, PAS, single-chain variable fragments, stimulus-responsive systems

Received: August 26, 2021
Revised: October 24, 2021
Published online: December 3, 2021

[1] T. M. Allen, C. Hansen, *Biochim. Biophys. Acta, Biomembr.* **1991**, *1068*, 133.
[2] D. Peer, J. M. Karp, S. Hong, O. C. Farokhzad, R. Margalit, R. Langer, *Nat. Nanotechnol.* **2007**, *2*, 751.
[3] E. Fleige, M. A. Quadir, R. Haag, *Adv. Drug Deliv. Rev.* **2012**, *64*, 866.
[4] E. Blanco, H. Shen, M. Ferrari, *Nat. Biotechnol.* **2015**, *33*, 941.
[5] A. Wörz, B. Berchtold, K. Moosmann, O. Prucker, J. Rühe, *J. Mater. Chem. B* **2012**, *22*, 19547.
[6] T. R. Hoare, D. S. Kohane, *Polymer* **2008**, *49*, 1993.
[7] C. J. Kearney, D. J. Mooney, *Nat. Mater.* **2013**, *12*, 1004.
[8] A. N. Zelikin, C. Ehrhardt, A. M. Healy, *Nat. Chem.* **2016**, *8*, 997.
[9] M.-T. Popescu, S. Mourtas, G. Pampalakis, S. G. Antimisiaris, C. Tsitsilianis, *Biomacromolecules* **2011**, *12*, 3023.
[10] B. E. B. Jensen, L. Hosta-Rigau, P. R. Spycher, E. Reimhult, B. Städler, A. N. Zelikin, *Nanoscale* **2013**, *5*, 6758.
[11] A. K. Gaharwar, N. A. Peppas, A. Khademhosseini, *Biotechnol. Bioeng.* **2014**, *111*, 441.
[12] P. Lavrador, M. R. Esteves, V. M. Gaspar, J. F. Mano, *Adv. Funct. Mater.* **2021**, *31*, 2005941.
[13] H. Hatakeyama, H. Akita, H. Harashima, *Adv. Drug Deliv. Rev.* **2011**, *63*, 152.
[14] H. Hatakeyama, H. Akita, H. Harashima, *Biol. Pharm. Bull.* **2013**, *36*, 892.
[15] M. C. Koetting, J. T. Peters, S. D. Steichen, N. A. Peppas, *Mater. Sci. Eng., R* **2015**, *93*, 1.
[16] S. Mura, J. Nicolas, P. Couvreur, *Nat. Mater.* **2013**, *12*, 991.
[17] N. Kamaly, B. Yameen, J. Wu, O. C. Farokhzad, *Chem. Rev.* **2016**, *116*, 2602.
[18] S. L. Pedersen, T. H. Huynh, P. Pöschko, A. S. Fruergaard, M. T. Jarlstad Olesen, Y. Chen, H. Birkedal, G. Subbiahdoss, E. Reimhult, J. Thøgersen, A. N. Zelikin, *ACS Nano* **2020**, *14*, 9145.
[19] R. Mo, T. Jiang, R. DiSanto, W. Tai, Z. Gu, *Nat. Commun.* **2014**, *5*, 3364.
[20] R. Mo, T. Jiang, Z. Gu, *Angew. Chem., Int. Ed.* **2014**, *53*, 5815.
[21] A. Matsumoto, T. Ishii, J. Nishida, H. Matsumoto, K. Kataoka, Y. Miyahara, *Angew. Chem., Int. Ed.* **2012**, *51*, 2124.
[22] K. R. Fruehauf, T. I. Kim, E. L. Nelson, J. P. Patterson, S.-W. Wang, K. J. Shea, *Biomacromolecules* **2019**, *20*, 2703.
[23] K. O'goshi, J. Serup, *Skin Res. Technol.* **2006**, *12*, 155.
[24] J. Zempleni, T. Kuroishi, *Adv. Nutr.* **2012**, *3*, 213.
[25] Institute of Medicine, *Dietary Reference Intakes: The Essential Guide to Nutrient Requirements*, National Academies Press, Washington, DC **2006**.
[26] S. L. Yankell, J. J. Loux, *J. Periodontol.* **1977**, *48*, 228.
[27] D. M. Mock, *J. Nutr.* **2017**, *147*, 1487.
[28] L. Chatenoud, J. A. Bluestone, *Nat. Rev. Immunol.* **2007**, *7*, 622.
[29] M. X. Sliwkowski, I. Mellman, *Science* **2013**, *341*, 1192.
[30] T. Miyata, N. Asami, T. Uragami, *Nature* **1999**, *399*, 766.
[31] J. F. Rippmann, M. Klein, C. Hoischen, B. Brocks, W. J. Rettig, J. Gumpert, K. Pfizenmaier, R. Mattes, D. Moosmayer, *Appl. Environ. Microbiol.* **1998**, *64*, 4862.
[32] L. Vaks, I. Benhar, in *Human Monoclonal Antibodies: Methods and Protocols* (Ed: M. Steinitz), Humana Press, Totowa, NJ **2014**, pp. 171–184.
[33] J. Lobstein, C. A. Emrich, C. Jeans, M. Faulkner, P. Riggs, M. Berkmen, *Microb. Cell Fact.* **2012**, *11*, 56.
[34] M. Schlapschy, U. Binder, C. Börger, I. Theobald, K. Wachinger, S. Kisling, D. Haller, A. Skerra, *Protein Eng., Des. Sel.* **2013**, *26*, 489.
[35] J. Breibeck, A. Skerra, *Biopolymers* **2018**, *109*, e23069.
[36] Y. Bavli, I. Winkler, B. M. Chen, S. Roffler, R. Cohen, J. Szebeni, Y. Barenholz, *J. Control. Release* **2019**, *306*, 138.
[37] T. J. Vaughan, A. J. Williams, K. Pritchard, J. K. Osbourn, A. R. Pope, J. C. Earnshaw, J. McCafferty, R. A. Hodits, J. Wilton, K. S. Johnson, *Nat. Biotech.* **1996**, *14*, 309.
[38] G. Pedrazzi, F. Schwesinger, A. Honegger, C. Krebber, A. Plückthun, *FEBS Lett.* **1997**, *415*, 289.
[39] A. Honegger, S. Spinelli, C. Cambillau, A. Plückthun, *Prot. Sci.* **2005**, *14*, 2537.
[40] F. Kohen, H. Bagci, G. Barnard, E. A. Bayer, B. Gayer, D. G. Schindler, E. Ainbinder, M. Wilchek, in *Methods in Enzymology*, Academic Press, Cambridge **1997**, pp. 451–463.
[41] P. Carter, L. Presta, C. M. Gorman, J. B. Ridgway, D. Henner, W. L. Wong, A. M. Rowland, C. Kotts, M. E. Carver, H. M. Shepard, *Proc. Natl. Acad. Sci. U. S. A.* **1992**, *89*, 4285.
[42] S. Jung, A. Plückthun, *Protein Eng., Des. Sel.* **1997**, *10*, 959.
[43] J. Willuda, A. Honegger, R. Waibel, P. A. Schubiger, R. Stahel, U. Zangemeister-Wittke, A. Plückthun, *Cancer Res.* **1999**, *59*, 5758.
[44] H. J. Wagner, W. Weber, M. Fussenegger, *Adv. Sci.* **2021**, *8*, 2004018.
[45] D. S. Bindels, L. Haarbosch, L. van Weeren, M. Postma, K. E. Wiese, M. Mastop, S. Aumonier, G. Gotthard, A. Royant, M. A. Hink, T. W. J. Gadella, *Nat. Methods* **2017**, *14*, 53.
[46] R. J. Gübeli, D. Hövermann, H. Seitz, B. Rebmann, R. G. Schoenmakers, M. Ehrbar, G. Charpin-El Hamri, M. Daoud-El Baba, M. Werner, M. Müller, W. Weber, *Adv. Funct. Mater.* **2013**, *23*, 5355.
[47] B. A. Kerwin, *J. Pharm. Sci.* **2008**, *97*, 2924.
[48] I. Sela-Culang, V. Kunik, Y. Ofran, *Front. Immunol.* **2013**, *4*, 302.
[49] M. W. Jones, G. Mantovani, S. M. Ryan, X. Wang, D. J. Brayden, D. M. Haddleton, *Chem. Commun.* **2009**, 5272.
[50] M. Hörner, K. Raute, B. Hummel, J. Madl, G. Creusen, O. S. Thomas, E. H. Christen, N. Hotz, R. J. Gübeli, R. Engesser, B. Rebmann, J. Lauer, B. Rolauffs, J. Timmer, W. W. A. Schamel, J. Pruszak, W. Römer, M. D. Zurbriggen, C. Friedrich, A. Walther, S. Minguet, R. Sawarkar, W. Weber, *Adv. Mater.* **2019**, *31*, 1806727.
[51] Y.-C. Chiu, M.-H. Cheng, H. Engel, S.-W. Kao, J. C. Larson, S. Gupta, E. M. Brey, *Biomaterials* **2011**, *32*, 6045.
[52] J. Yu, X. Xu, F. Yao, Z. Luo, L. Jin, B. Xie, S. Shi, H. Ma, X. Li, H. Chen, *Int. J. Pharm.* **2014**, *470*, 151.
[53] H. HogenEsch, D. T. O'Hagan, C. B. Fox, *npj Vaccines* **2018**, *3*, 51.
[54] M. S. Rehmann, K. M. Skeens, P. M. Kharkar, E. M. Ford, E. Maverakis, K. H. Lee, A. M. Kloxin, *Biomacromolecules* **2017**, *18*, 3131.
[55] P. S. Uster, T. M. Allen, B. E. Daniel, C. J. Mendez, M. S. Newman, G. Z. Zhu, *FEBS Lett.* **1996**, *386*, 243.
[56] S. Jalota, S. B. Bhaduri, A. C. Tas, *Mater. Sci. Eng., C* **2008**, *28*, 129.
[57] G. Haran, R. Cohen, L. K. Bar, Y. Barenholz, *Biochim. Biophys. Acta* **1993**, *1151*, 201.
[58] B. L. Ellis, M. L. Hirsch, J. C. Barker, J. P. Connelly, R. J. Steininger, M. H. Porteus, *Virol. J.* **2013**, *10*, 74.
[59] A. Westhaus, M. Cabanes-Creus, A. Rybicki, G. Baltazar, R. G. Navarro, E. Zhu, M. Drouyer, M. Knight, R. F. Albu, B. H. Ng, P. Kalajdzic, M. Kwiatek, K. Hsu, G. Santilli, W. Gold, B. Kramer, A. Gonzalez-Cordero, A. J. Thrasher, I. E. Alexander, L. Lisowski, *Hum. Gene Ther.* **2020**, *31*, 575.
[60] M. Kunes, J. Kvetina, J. Malakova, J. Bures, M. Kopacova, S. Rejchrt, *Neuroendocrinol. Lett.* **2010**, *31*, 57.
[61] E. Belykh, N. R. Onaka, X. Zhao, I. Abramov, J. M. Eschbacher, P. Nakaji, M. C. Preul, *Front. Neurol.* **2021**, *12*, 1169.
[62] F. Acerbi, C. Cavallo, M. Broggi, R. Cordella, E. Anghileri, M. Eoli, M. Schiariti, G. Broggi, P. Ferroli, *Neurosurg. Rev.* **2014**, *37*, 547.

[63] F. Acerbi, M. Broggi, K.-M. Schebesch, J. Höhne, C. Cavallo, C. D. Laurentis, M. Eoli, E. Anghileri, M. Servida, C. Boffano, B. Pollo, M. Schiariti, S. Visintini, C. Montomoli, L. Bosio, E. L. Corte, G. Broggi, A. Brawanski, P. Ferroli, *Clin. Cancer Res.* **2018**, *24*, 52.
[64] L. P. S. Paul, D. Debruyne, D. Bernard, D. M. Mock, G. L. Defer, *Expert Opin. Drug Metab. Toxicol.* **2016**, *12*, 327.
[65] W. Weber, J. Stelling, M. Rimann, B. Keller, M. D.-E. Baba, C. C. Weber, D. Aubel, M. Fussenegger, *Proc. Natl. Acad. Sci. U. S. A.* **2007**, *104*, 2643.
[66] G. Finak, J. Frelinger, W. Jiang, E. W. Newell, J. Ramey, M. M. Davis, S. A. Kalams, S. C. De Rosa, R. Gottardo, *PLoS Comput. Biol.* **2014**, *10*, e1003806.
[67] X. Xiao, J. Li, R. J. Samulski, *J. Virol.* **1998**, *72*, 2224.
[68] D. Grimm, A. Kern, M. Pawlita, F. Ferrari, R. Samulski, J. Kleinschmidt, *Gene Ther.* **1999**, *6*, 1322.
[69] E. Monsellier, H. Bedouelle, *Protein Eng., Des. Sel.* **2005**, *18*, 445.
[70] C. Ritz, F. Baty, J. C. Streibig, D. Gerhard, *PLoS One* **2015**, *10*, e0146021.
[71] R. Core Team, *R: A Language and Environment for Statistical Computing*, R Foundation For Statistical Computing, Vienna, Austria **2021**.